Journal of Solid State Chemistry **163,** 294–299 (2002)
doi:10.1006/jssc.2001.9411, available online at http://www.idealibrary.com on IDEAL®

Order–Disorder Structural Phase Transitions in Alkali Perchlorates

Jianjun Liu,*,†,[1] Chun-gang Duan,† W. N. Mei,† R. W. Smith,‡ and J. R. Hardy*

*Department of Physics and Center for Electro-Optics, University of Nebraska, Lincoln, Nebraska 68588-0111; †Department of Physics, University of Nebraska, Omaha, Nebraska 68182-0266; and ‡Department of Chemistry, University of Nebraska, Omaha, Nebraska 68182-0109

Received June 15, 2001; in revised form September 20, 2001; accepted September 27, 2001

Order–disorder structural phase transitions in alkali perchlorates $M\mathrm{ClO_4}$ (M = Na, K, Rb, Cs) are investigated using molecular dynamics simulation. The potentials in the simulations are based on the Gordon–Kim modified electron gas formalism extended to molecular ions. The simulations yield first-order phase transitions in perchlorates from low temperature orthorhombic structures to high temperature cubic NaCl structures. The perchlorate ions are found to be orientational disordered in the high temperature phases. © 2002 Elsevier Science

Key Words: **alkali perchlorate; molecular-dynamics simulation; phase transition; Gordon–Kim potential; order–disorder.**

INTRODUCTION

Alkali perchlorates $M\mathrm{ClO_4}$ (M = Na, K, Rb, Cs) undergo order–disorder phase transitions at high temperature characterized by orientational disorder of perchlorate ions (1). At room temperature, $\mathrm{KClO_4}$, $\mathrm{RbClO_4}$, and $\mathrm{CsClO_4}$ crystallize in the same orthorhombic lattice with space group *Pnma* (2, 3), while $\mathrm{NaClO_4}$ has a *Cmcm* orthorhombic symmetry (4). They all have cubic NaCl structure with space group *Fm*3*m* at high temperature (5). The reported transition temperatures T_c are 581, 574, 548, and 482 K for $\mathrm{NaClO_4}$, $\mathrm{KClO_4}$, $\mathrm{RbClO_4}$, and $\mathrm{CsClO_4}$, respectively (5). Experimental studies on these perchlorates have been carried out extensively by a variety of techniques (6–16). The phase transitions were attributed to the reorientation of $\mathrm{ClO_4}$ ions.

Affouard and Depondt studied the phase transition in $\mathrm{KClO_4}$ by molecular dynamics (MD) based on classical potentials (17, 18). They reproduced the correct structures in both the low-temperature ordered phase and the high-temperature orientationally disordered phase, and found that the $\mathrm{ClO_4}$ ions have preferred orientations of T_d symmetry with orientational disorder in the high temperature phase. There are no theoretical studies on the phase transitions in $\mathrm{NaClO_4}$, $\mathrm{RbClO_4}$, and $\mathrm{CsClO_4}$ to date.

[1] To whom correspondence should be addressed. Fax: 402-472-2879. E-mail: jliu@unlserve.unl.edu.

To understand better the nature of the structural phase transitions in the alkali perchlorates mentioned above, we investigate the phase transitions by molecular dynamics simulation using first-principle potentials. We focus on how the structures of alkali perchlorates transform from orthorhombic to cubic, which was not stressed in Refs. (17) and (18), by monitoring the cross-sections of the average structures and the atom–atom radial distribution functions at different temperatures. We use the Gordon–Kim modified electron-gas model (19) to calculate interionic interactions, and *Taylor* expansions of the molecular ion's energy to describe the covalent intraionic interactions in the molecular ion ($\mathrm{ClO_4}$). This method leads to a first-principle description of the potential-energy surfaces for ionic molecular crystals (20).

INTER- AND INTRAMOLECULAR POTENTIALS AND STATIC RELAXATION

Our MD simulation originates from the Gordon–Kim model for ionic crystals. It was extended to deal with ionic molecular crystals, such as $\mathrm{K_2SeO_4}$, in which strong covalency exists within the molecular ion ($\mathrm{SeO_4}$) (20). We use the same method to study alkali perchlorates which consist of alkali cations (Na, K, Rb, Cs) and molecular anions ($\mathrm{ClO_4}$). The main idea is that, since the interactions within the same $\mathrm{ClO_4}$ ion are covalent, and those between different $\mathrm{ClO_4}$ ions are ionic, the intraionic and interionic interactions are considered separately.

Specifically, we first performed *ab initio* quantum-chemistry calculation for the whole $\mathrm{ClO_4}$ ion to obtain the optimized structure and the electron charge densities of each individual atom (Cl and O) from the electron charge densities of whole $\mathrm{ClO_4}$ ion in the spirit of a Mulliken population analysis (21). Then, the numerical short-range pair potentials between different $\mathrm{ClO_4}$ ions and between alkali ions and $\mathrm{ClO_4}$ ions were calculated from the resultant charge densities, together with those of the alkali ions according to Gordon–Kim electron-gas model (19). The tabulated charge densities of $\mathrm{Na^+}$, $\mathrm{K^+}$, and $\mathrm{Rb^+}$ were used

0022-4596/02 $35.00

TABLE 1
Theoretical Relaxed Structural Parameters of Alkali Perchlorates with Room Temperature Crystal Structure Symmetry Constraints

Crystal/Space group	$KClO_4$/*Pnma*	$RbClO_4$/*Pnma*	$CsClO_4$/*Pnma*	$NaClO_4$/*Cmcm*
a (Å)	8.2756 (8.765)	8.6993 (9.252)	9.5741 (9.823)	6.8017 (7.085)
b (Å)	5.7270 (5.620)	5.8298 (5.789)	5.8433 (6.009)	6.3369 (6.526)
c (Å)	7.0410 (7.205)	7.2736 (7.472)	7.4484 (7.764)	6.6397 (7.048)
x/*a* of alkali atom	0.1748 (0.18038)	0.1775 (0.18262)	0.2006 (0.18888)	0.00 (0.00)*
y/*b* of alkali atom	0.25 (0.25)*	0.25 (0.25)*	0.25 (0.25)*	0.6214 (0.6637)
z/*c* of alkali atom	0.3407 (0.33865)	0.1577 (0.16327)	0.1534 (0.16293)	0.25 (0.25)*
x/*a* of Cl	0.0611 (0.06954)	0.0627 (0.0654)	0.0257 (0.0561)	0.00 (0.00)*
y/*b* of Cl	0.25 (0.25)*	0.25 (0.25)*	0.25 (0.25)*	0.1410 (0.1683)
z/*c* of Cl	0.8234 (0.81160)	0.6787 (0.6916)	0.7002 (0.6956)	0.25 (0.25)*
x/*a* of O(1)	0.1904 (0.19372)	0.1852 (0.1804)	0.0919 (0.1577)	0.00 (0.00)*
y/*b* of O(1)	0.25 (0.25)*	0.25 (0.25)*	0.25 (0.25)*	0.2741 (0.2989)
z/*c* of O(1)	0.9610 (0.94289)	0.5447 (0.5641)	0.5257 (0.5651)	0.0727 (0.0867)
x/*a* of O(2)	−0.0926 (−0.0741)	−0.0843 (−0.0715)	−0.1247 (−0.0782)	0.1734 (0.1638)
y/*b* of O(2)	0.25 (0.25)*	0.25 (0.25)*	0.25 (0.25)*	0.0086 (0.0384)
z/*c* of O(2)	0.9206 (0.90607)	0.5862 (0.6051)	0.6796 (0.6257)	0.25 (0.25)*
x/*a* of O(3)	0.0729 (0.08098)	0.0749 (0.0784)	0.0674 (0.0741)	
y/*b* of O(3)	0.0435 (0.04086)	0.0475 (0.0488)	0.0480 (0.0551)	
z/*c* of O(3)	0.7060 (0.69491)	0.7927 (0.8025)	0.7990 (0.8015)	

Note. Experimental values are given in parentheses; (*) fixed by crystal structure symmetry.

(22), while those for Cs^+ were calculated with the software of Liberman *et al.* (23). The numerical short-range potentials were then fitted to the analytic form $U(r) = e^{-\alpha r}\sum_{n=0}^{N} C_n r^{m+n}$, $r_c < r < r_t$, with $r_c = 2$ atomic unit (a.u.), $r_t = 12$ a.u., $N = 8$. To complete the fit, a core function $U(r) = A + B/r^6$, $r \le r_c$, and a tail function $U(r) = D\exp(-\beta r^2)$, $r \ge r_t$ were attached by requiring that the potential and its first derivative be continuous at the points of attachment. There are 15 fitted coefficients A, B, m, α, C_n, D, β for each pair potential. The authors will be pleased to provide listings of potential parameters to anyone interested.

The interaction potentials within the ClO_4 ion were described by a harmonic expansion of the energy in terms of bond lengths, bond angles, and dihedral angles. The long-range Coulomb interactions were calculated using the Mulliken charges of the Cl and O atoms, specifically, +1.96852 for Cl and −0.74213 for O. The ionic charge for the alkali ions is +1.

We used GAUSSIAN94 commercial package (24) to perform an *ab initio* quantum-chemistry calculation for ClO_4 ion by using the standard 6-31G** basis set for Cl and O atoms. The force constants of the harmonic expansion were also calculated from GAUSSIAN94.

We used the interaction potentials as obtained to perform static relaxation calculations for all four alkali perchlorates with room temperature crystal structure symmetry constraints. This procedure determines the positions of the atoms and the lattice vectors that correspond to the minimum of the theoretical potential energy surface. The periodic boundary conditions, a Newton–Raphson algorithm, and the standard technique of the Ewald sum were used in calculating the lattice energy and forces.

The parameters for the relaxed structures of four alkali perchlorates along with the room temperature experimental values (2–4) are given in Table 1. From this table, one can see that agreement between the lattice constants is within 6% for all perchlorates. The discrepancies in fractional atomic positions are comparable with the typical thermal fluctuation of the atomic position at room temperature. Overall comparison of relaxed structures and experimental structures provides a sensitive test of the validity of the theoretical potential-energy surfaces. The reasonable agreements of our relaxed structures with the experimental structures indicate that our potentials provide a good representation of the interactions in the alkali perchlorates investigated.

MOLECULAR-DYNAMIC SIMULATIONS OF THE PHASE TRANSITIONS

Our molecular dynamics simulations started from the theoretical relaxed structures. We used a supercell with 192 atoms which was formed by doubling the orthorhombic unit cells in all three directions. Our simulations follow a constant (-zero) pressure algorithm (25) with periodic boundary conditions and Ewald summation for lattice energy and forces. The molecular-dynamics time step used was 0.001 ps. At each temperature the averages of the ion positions, energy, etc., were taken over 10 ps.

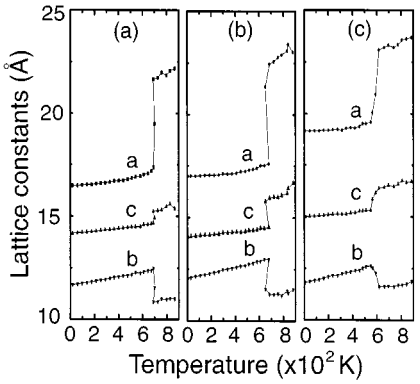

FIG. 1. Lattice constants as a function of temperature for the MD runs on (a) $KClO_4$, (b) $RbClO_4$, and (c) $CsClO_4$.

a. Phase Transitions in $KClO_4$, $RbClO_4$, and $CsClO_4$

Figure 1 presents lattice constants as a function of temperature for the MD runs on $KClO_4$, $RbClO_4$, and $CsClO_4$. It clearly shows that $KClO_4$, $RbClO_4$, and $CsClO_4$ exhibit similar first order phase transitions at 672, 654, and 573 K, respectively. The theoretical transition temperatures are 18% higher than experimental values. Both lattice constants a and c expand at the transition but lattice constant a has a larger expansion, while lattice constant b contracts at the transition. Above the phase transition, $a/\sqrt{2} \cong \sqrt{2}b \cong c \cong a_{cubic}$, where a_{cubic} is the cubic lattice constant. The theoretical volume changes at the transition are about 13% for all perchlorates, in agreement with the experimental values of 12%.

In order to examine how the phase transitions take place, Figs. 2 and 3 show the cross-sections of the average structures of $KClO_4$ along the [001] (c axis) and [100] (a axis) directions of the orthorhombic supercell at four different temperatures. In the plots the lines connect the chlorine atoms with their nearest oxygen atoms and the isolated ellipses represent the K atoms. Large ovals centered about atoms represent "thermal ellipsoids" which indicate the r.m.s. deviation of the atoms from their average positions. Figure 4 presents changes of atom–atom radial distribution functions of $KClO_4$ with temperature.

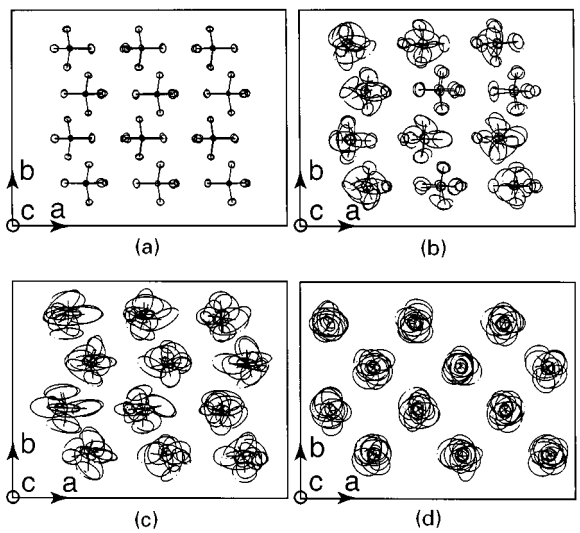

FIG. 2. Projections of the atomic positions along the orthorhombic c axis in the average structure of $KClO_4$ obtained from the MD simulation. (a) 363 K, (b) 550 K, (c) 650 K, (d) 690 K.

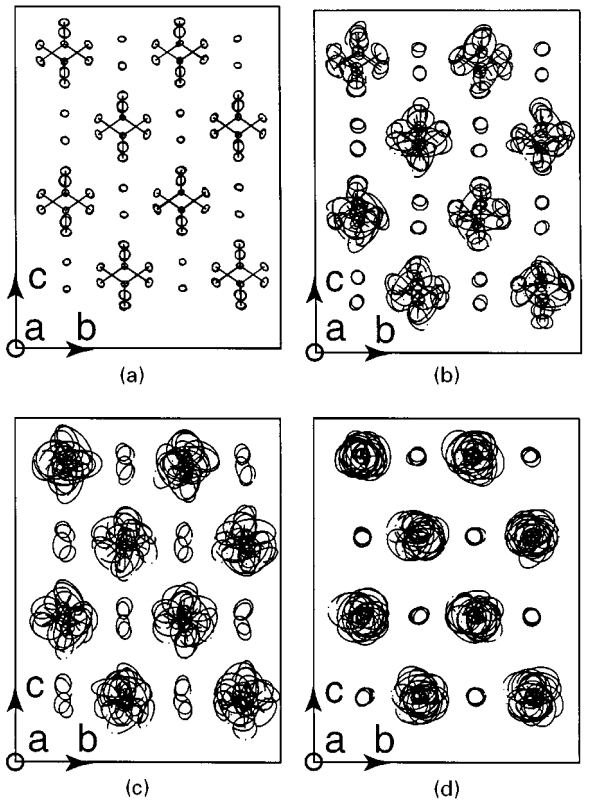

FIG. 3. Projections of the atomic positions along the orthorhombic a axis in the average structure of $KClO_4$ obtained from the MD simulation. (a) at 363 K, (b) 550 K, (c) 650 K, (d) 690 K.

It can be seen from Figs. 2a and 3a that, at low temperature, the orientations of the ClO_4 ions are perfectly ordered. The K–Cl, K–K, Cl–Cl, and K–O distribution functions contain many narrow, sharp peaks as shown in Fig. 4a. As the temperature increases the orientations of ClO_4 ions become partially disordered (Figs. 2b and 3b). The thermal ellipsoids of the O atoms show that some ClO_4 ions deviate their original orientations. The orientational disorder of the ClO_4 ions makes the peaks in K–O distribution function smeared (Fig. 4b). The thermal motions of the K and Cl atoms also increase so that the sharp peaks in K–Cl, K–K, and Cl–Cl distribution functions are merging with increasing temperature (Fig. 4b).

Figures 2c and 3c are projections of the average structure just below the transition. They show that the structure is in

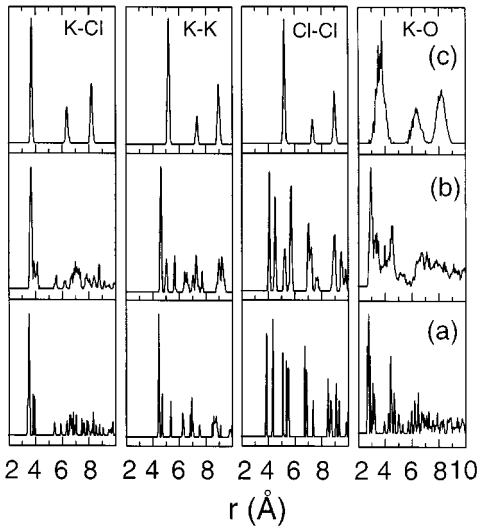

FIG. 4. Atom–atom radial distribution function of $KClO_4$ in the average structure obtained from the MD simulation. Row (a), at 363 K; Row (b), at 550 K; Row (c), at 690 K.

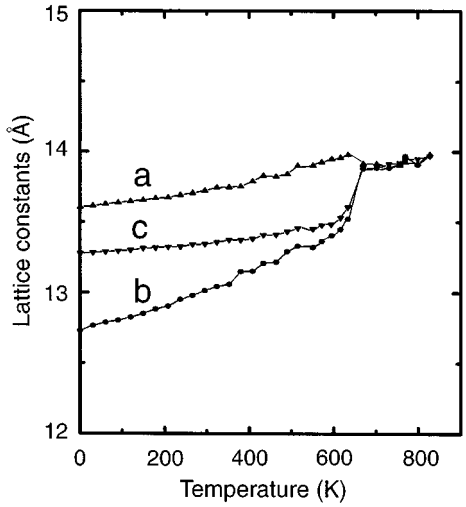

FIG. 5. Lattice constants as a function of temperature for the MD run on $NaClO_4$.

change. The thermal ellipsoids of the K and ClO_4 ions indicate that the K and ClO_4 ions are shifting along the *a* and *c* axes. After the transition, the lattice transforms into a cubic structure as shown in Figs. 2d and 3d. The orientations of the ClO_4 ions become completely isotropic above the transition temperature. The K–Cl, K–K, and Cl–Cl distribution functions indicate that K and Cl atom sublattices form a NaCl structure, while the peaks in the K–O distribution function evolve to three broad bands in the $0 \sim 10$ Å range (Fig. 4c). From our simulation we find that the [100] (*a* axis) and [001] (*c* axis) directions of the orthorhombic cell transform to the [110] and [001] directions of the NaCl structure, respectively.

The mechanism of the phase transitions in $RbClO_4$ and $CsClO_4$ is the same as that in $KClO_4$ described above. The counterparts for $RbClO_4$ and $CsClO_4$ are similar to those in Figs. 2, 3, and 4.

b. Phase Transition in $NaClO_4$

The lattice constants as a function of temperature for the MD run on $NaClO_4$ are shown in Fig. 5. The phase transition occurs at 670 K compared with the experimental value 581 K. Below the transition temperature, all the lattice constants *a*, *b*, and *c* expand, with lattice constant *b* having a large expansion coefficient. At the transition point, three orthorhombic lattice constants equal each other and change to cubic lattice constants. The phase transition is associated with a 12.8% change in the volume.

The cross-sections of the average structures of $NaClO_4$ along the [100] (*a* axis) and [011] directions of the orthorhombic supercell at different temperatures are shown in Figs. 6 and 7. Again, large ovals centered about atoms represent "thermal ellipsoids" and the isolated ellipses represent the Na atoms. Figure 8 is the atom–atom radial distribution functions of $NaClO_4$ at different temperatures.

Comparing Figs. 6 and 7 with Figs. 2 and 3, one finds that the disordering process of ClO_4 ions in $NaClO_4$ is similar to that in $KClO_4$. Specifically, the ClO_4 ions in $NaClO_4$ are orientational ordered at low temperature (Figs. 6a and 7a). At higher temperature, the large thermal ellipsoids of the O atoms indicate onset of the orientational disorder of the ClO_4 (Figs. 6b and 7b). Figures 6c and 7c are projections of

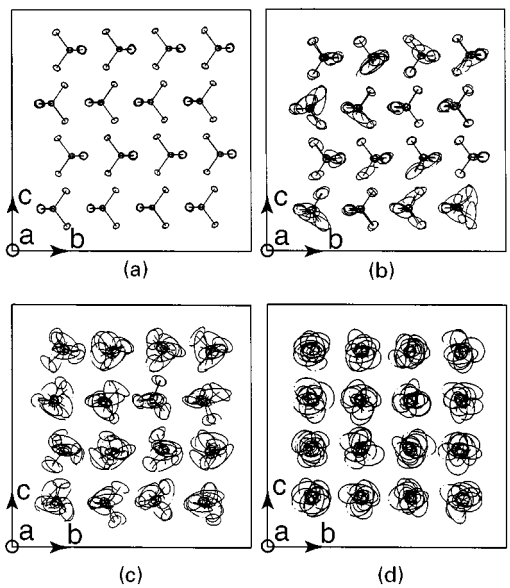

FIG. 6. Projections of the atomic positions along the orthorhombic *a* axis in the average structure of $NaClO_4$ obtained from the MD simulation: (a) 380 K, (b) 540 K, (c) 650 K, (d) 695 K.

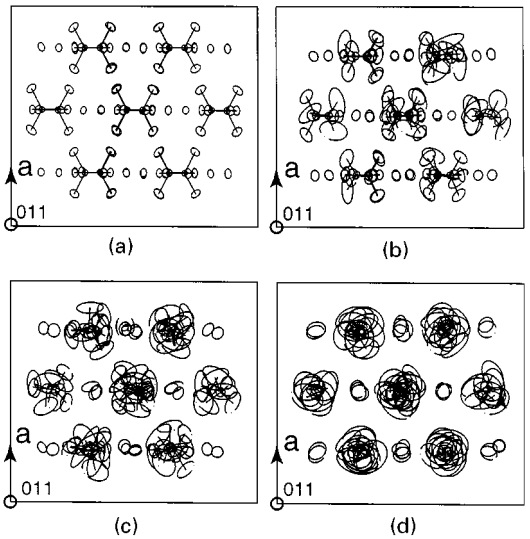

FIG. 7. Projections of the atomic positions along the orthorhombic [011] direction in the average structure of $NaClO_4$ obtained from the MD simulation. (a) 380 K, (b) 540 K, (c) 650 K, (d) 695 K.

the average structure just below the transition. As in the case of $KClO_4$, the thermal ellipsoids of the Na and ClO_4 ions indicate that the Na and ClO_4 ions are displacing along the *b* axis. The structure of $NaClO_4$ transforms to a cubic structure above the transition temperature and the ClO_4 ions have random orientations (Figs. 6d and 7d).

The radial distribution functions shown in Fig. 8 also show the orientational disorder of the ClO_4 ions and the displacements of the Na and ClO_4 ion sublattice. At high temperature, the narrow peaks in radial distribution functions merge into broader peaks. The distribution functions of $NaClO_4$ are similar to those of $KClO_4$ above the phase transition, which indicates that the high temperature structure of $NaClO_4$ is also NaCl structure. The relationship between the orthorhombic and cubic structure of $NaClO_4$ is that the three orthorhombic axes *a*, *b*, and *c* transform to three cubic axes [100], [010], and [001], respectively.

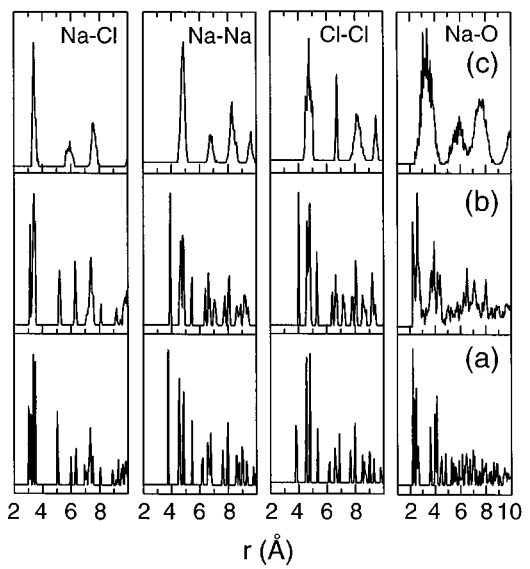

FIG. 8. Atom–atom radial distribution function of $NaClO_4$ in the average structure obtained from the MD simulation. Row (a), at 380 K; Row (b), at 540K; Row (c), at 695 K.

DISCUSSION

To explain Raman light scattering of $KClO_4$, Toupry *et al.* (9) proposed a model with the relationship between the low and high temperature crystal axes shown in Fig. 9a. However, a neutron scattering experiment contradicted the above model (16). A simple relation could not be found between the orientations of the orthorhombic and cubic crystals. The authors concluded that when going from the less symmetric to the more symmetric phase, the strong first-order character of the transition impedes any relationship between the two structures. A direct observation of the phase transition on a microscopic scale from our simulation shows that the transition in $KClO_4$ follows the simple mechanism proposed by Toupry *et al.* (9). The simulation based on the classical potentials and a rigid-molecule model obtained the same result (18). The authors argued that the model shown in Fig. 9a is microscopically correct. However, the behavior of the real sample, which is presumably connected with the large volume increase at the transition, is driven by effects on a nonmicroscopic scale. We think that the phase transition of $KClO_4$ in reality might start from the nucleation sites. As there are no constraints for the high temperature phase to follow the orientation of the low temperature phase, the nucleation is random with no preferred orientation. As a result, the orientation of lattice vector of the high temperature phase might be different from those predicted from the low temperature phase, whereas, in our simulation, the high temperature phase must have some relationship with the low temperature phase due to the periodic boundary condition constraints.

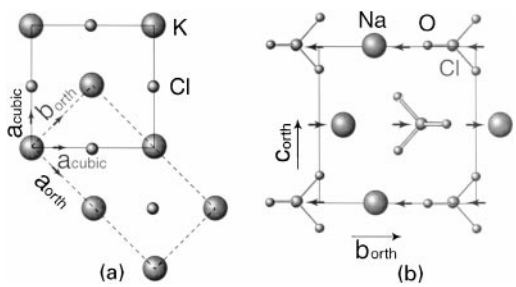

FIG. 9. Structure relationship between orthorhombic phase and the cubic phase. (a) $KClO_4$, (solid lines) cubic; (dashed lines) orthorhombic. (b) $NaClO_4$, only $x = 0$ plane is shown. The arrows indicate the displacements of Na and ClO_4 ions in the orthorhombic phase from their positions in the cubic phase.

Our simulation reveals the same microscopic mechanism of phase transition in $KClO_4$ as that in Ref. (18). However, our first-principle potentials, which are based on the density function theory and the Gordon–Kim model, are totally different from the empirical potentials and the rigid-molecule model in (18). The same phase transition mechanism is achieved by two different methods making it more credible.

For the phase transition in $NaClO_4$ our simulation agrees with the X-ray study (13). The structural relation of the orthorhombic phase to the cubic phase is illustrated in Fig. 9b by taking the face centered cubic cell. The positions of Na and ClO_4 ions in the orthorhombic phase are displaced from their positions in the cubic phase as indicated by arrows. It is clear from our simulation that the phase transition is associated with displacements of ions as well as the reorientation of ClO_4 ions. From Figs. 6a and 9b, one can see that the distortion of orthorhombic phase from the cubic phase mainly results from the displacements of Na and ClO_4 ions along the *b* direction, which leads to the orthorhombic lattice constant *b* having the smallest value. As the orthorhombic phase transforms to the cubic phase, Na and ClO_4 ions have to make large displacements along the *b* direction to decrease the distortion, thus, the lattice constant *b* have a larger expansion coefficient than lattice constants *a* and *c*.

A simple relationship between the high temperature cubic phase and the low temperature orthorhombic phase exists in our simulation that the sublattice of alkali metal and the chlorine ions in orthorhombic phases is distorted cubic NaCl structure. Since the distortions are only due to the displacements of alkali metal and the chlorine ions, the radial distribution functions of the alkali metal and the chlorine do not show significant changes as the structure transforms from the orthorhombic phase to cubic phase. On the other hand, the distribution functions of the alkali metal and the oxygen change drastically because of the orientational disorder of the ClO_4 ions.

Because we did not adjust any potential parameters in our simulation, we must take what phase transition temperature T_c the simulation gives us. There might be some shortcomings in our potentials, which led to the high T_c. We found if we decreased the long-range Coulomb interactions by reducing the electronic charge of the alkali-metal ion and the O ions, the T_c would approach the experimental values. This implies that the long-range Coulomb interactions might be too strong in our simulation; whereas, the volume change agreement with the experiment might mean the short-range force is accurate.

ACKNOWLEDGMENTS

This work was supported by the U.S. Army Research Office under Grant Nos. DAAG 55-97-1-0106 and DAAG 55-98-1-0273. The computer facility was supported by Nebraska-EPSCoR-NSF Grant EPS-9720643.

REFERENCES

1. C. N. R. Rao and B. Prakash, *Rep. NSRDS- Nat. Bur. Standards* **56,** 22 (1975).
2. J. W. Bats and H. Fuess, *Acta Crystallogr., Sect. B: Struct. Sci.* **38,** 2116 (1982).
3. J. Granzin, *Z. Kristallogr.* **184,** 157 (1988).
4. R. Wartchow and H. J. Berthold, *Z. Kristallogr.* **147,** 307 (1978).
5. N. G. Parsonage and L. A. K. Staveley, "Disorder in Crystals." Clarendon Press, Oxford, 1978.
6. T. Shripathi, H. L. Bhat, and P. S. Narayanan, *Phys. Status Solidi A* **126,** 511 (1991).
7. G. Raghurama, T. A. Al-Dhahir, and H. L. Bhat, *J. Phys. C* **20,** 4505 (1987).
8. S. Seetharaman, H. L. Bhat, and P. S. Narayanan, *Indian J. Phys. B* **58,** 294 (1984).
9. N. Toupry, H. Poulet, M. Le Postollec, R. M. Pick, and M. Yvinec, *J. Raman Spectrosc.* **14,** 166 (1983)
10. V. N. Belomestnykh, *Inorg. Mater.* **18,** 399 (1982).
11. S. K. Syal and S. R. Yoganarasimhan, *Indian J. Chem. A* **15,** 852 (1977).
12. S. K. Syal and S. R. Yoganarasimhan, *J. Solid State Chem.* **10,** 332 (1974).
13. S. Yamamoto and Y. Shinnaka, *J. Phys. Soc. Jpn.* **52,** 3080 (1983).
14. H. D. Lutz, R. A. Becker, B. G. Kruska, and H. J. Berthold, *Spectrochim. Acta A* **35,** 797 (1979).
15. N. Toupry-Krauzman and H. Poulet, *J. Raman Spectrosc.* **7,** 1 (1978).
16. B. Denise, M. Debeau, Ph. Depondt, and G. Heger, *J. Phys.* (*Paris*) **49,** 1203 (1988)
17. F. Affouard and Ph. Depondt, *J. Phys. I, France* **6,** 149 (1996).
18. F. Affouard and Ph. Depondt, *Europhys. Lett.* **33,** 365 (1996).
19. R. G. Gordon and Y. S. Kim, *J. Chem. Phys.* **56,** 3122 (1972).
20. H. M. Lu and J. R. Hardy, *Phys. Rev. B* **42,** 8339 (1990).
21. R. S. Mulliken, *J. Chem. Phys.* **23,** 1833 (1955).
22. E. Clementi and C. Roetti, *At. Data Nucl. Data Tables* **14,** 177 (1974).
23. D. A. Liberman, D. T. Cromer, and J. T. Waber, *Comput. Phys. Commun.* **2,** 107 (1971).
24. M. J. Frish, *et al.*, "GAUSSIAN94." Gaussian, Inc., Pittsburgh, PA, 1994.
25. M. Parrinello and A. Rahman, *Phys. Rev. Lett.* **45,** 1196 (1980).